Experimental UAV-Aided RSSI Localization of a Ground RF Emitter in 865 MHz and 2.4 GHz Bands

Stefano Moro, Vineeth Teeda, Davide Scazzoli, Luca Reggiani, Maurizio Magarini
Politecnico di Milano, Italy. Email: (firstname.lastname)@polimi.it

***Abstract*—Unmanned Aerial Vehicles (UAVs) can be used as low altitude platforms in several applications. In this paper, we propose their use to localize a ground Radio Frequency (RF) emitter by collecting measures of the Received Signal Strength Indicator (RSSI) at different positions. The main contribution of the work consists in the definition of an experimental setup for the simultaneous measures of RSSI and receiver position. The RSSI is measured by an actual transceiver, the Adalm Pluto Software Defined Radio (SDR) development board, programmed with the open-source software GNU Radio. The position is provided by GPS and Inertial Measuring Unit (IMU) sensors on the drone. The measures are acquired in the $865\,\mathrm{MHz}$ Short Range Device (SRD) and $2.4\,\mathrm{GHz}$ Industrial Scientific Medical (ISM) unlicensed frequency bands. Since the ISM measures can be affected by interference generated by different sources (e.g. Wi-Fi access points and UAV controller), the SRD band is exploited for collecting the RSSI measures with less interference. A maximum likelihood (ML) algorithm is applied to the collected data for estimating the transmitter location. For the considered setup we show that the mean absolute localization error is around $4\,\mathrm{m}$ without interference and $5\,\mathrm{m}$ with interference. A threshold-based technique is proposed to improve the accuracy in presence of interference.**

***Index Terms*—Unmanned Aerial Vehicles (UAVs), Received Signal Strength Indicator (RSSI), Software Defined Radio (SDR), Localization, Interference.**

I. Introduction

Unmanned Aerial Vehicles (UAVs) are revolutionizing the telecommunication industry thanks to their mobility. They find applications in the fast on-demand deployment of aerial base stations and in search and rescue operations [1]. In such applications, the localization of ground targets is often a helpful feature or even a critical requirement [2]. For instance, in search and rescue operations the possibility of re-establishing the connectivity and localizing the ground terminals can save lives by accelerating the search activities and saving the workforce for the rescue activities. In general, the localization of targets can be classified as *passive* or *active*: in passive localization, targets do not emit signals useful for their position estimates and they are typically localized by employing radar, lidar, or other sensing technologies while, in active localization, targets emit Radio Frequency (RF) signals [3].

Given the wide availability of hardware (HW) equipment capable of measuring the Received Signal Strength Indicator (RSSI), active localization of RF transmitters is largely used in practical systems [2], [4]–[7]. However, other approaches can be adopted to tackle the localization problem: Time of Arrival (ToA) [8], Time Difference of Arrival (TDoA) [9], and Angle of Arrival (AoA) [10] are the main exemplary techniques. It is worth noting that all of them require more complex and heavier HW in comparison to RSSI, thus increasing computational complexity and total weight, which is a critical constraint for UAV applications. On the other hand, an aerial platform based on pure RSSI, or difference of RSSI [11], can be implemented with much simpler HW and even the simplest Wireless Sensor Network (WSN) nodes are typically able to measure it [4], [7].

A. Related Work

In recent years, researchers have deeply investigated the deployment of UAVs for the localization of a ground RF transmitter. In the simulation study [5] a UAV is used as an anchor point in the localization process and its measures are mixed with those obtained from ground anchor nodes for localizing a ground emitter. In [6], it is studied a localization method where three fixed-wing UAVs cooperate for scanning a wide area of $10 \times 10\,\mathrm{km}^2$ and looking for an RF emitter with unknown transmit power. On the other hand, articles that tackle RSSI localization in the presence of interference focus mainly on indoor scenarios, with solutions often based on measures taken from multiple directional antennas [12] or on the use of frequency hopping capability to avoid the interference [13].

There are not so many experimental works that implement RSSI-based localization and only a few of them exploit UAVs as anchor points. In [7] a ground RF emitter localization is implemented deploying multiple ground anchor nodes based on ZigBee transceivers. Others exploit the capability of the UAVs for the localization process but use the collected data to understand how to manoeuvre the drone [14], [15]. In [14], front and rear-facing directional antennas are mounted on the UAV to localize and move towards the ground RF emitter by comparing the RSSI from the two antennas. In [15], many directional antennas connected to a single receiver with a fast switch sense the power. The implementation of this strategy allows for a fast estimation of the bearing of the ground RF transmitter and move towards it.

B. Main Contributions

In this paper, we present an experimental UAV platform for RSSI-based localization. RSSI measures are taken in different positions from the $2.4\,\mathrm{GHz}$ Industrial Scientific Medical (ISM) band. A Maximum Likelihood (ML) approach is applied to the collected data for offline localization of the ground RF emitter.

The accuracy of localization at 2.4 GHz can be affected by sporadic interference, which may come, for example, from nearby WiFi transmissions or the remote controller. To overcome this problem, a threshold-based RSSI technique is proposed. For validating the accuracy without strong interference, the 865 MHz band is also considered. Note that the two frequency bands are available for unlicensed use nearly worldwide. Moreover, we have performed a set of flights in the 865 MHz band with 3 transmitters on the ground to verify further the potential of our localization procedure.

Our work differs from others in the literature of RSSI-based UAV localization since it considers scenarios with and without interference. To the best of the authors' knowledge, this aspect was not investigated before with an experimental validation. Our approach is based on a single omnidirectional antenna connected to an ADALM-Pluto, a low-cost SDR board [16]. Furthermore, we provide a baseline localization algorithm through ML estimation based on multi-lateration, taking into account the impact of WiFi interference and providing a threshold-based solution to mitigate its impact on RSSI ranging. Differently from the interference management approach in [12], ours does not require directional antennas and additional HW, so reducing the weight and complexity of UAV operations.

C. Organization

Section II introduces the scenario with focus on the path loss model, the interference mitigation through a threshold, and the ML localization algorithm. Section III describes the measurement campaign carried out to gather the RSSI values, including the UAV path control. Sec. IV presents the localization results, with a specific focus on the target position estimation using the threshold-based technique. Finally Sec. V concludes the paper and discusses briefly the future work.

II. System model

A. Path Loss Model

The signal attenuation is related to the RSSI through the path loss model, expressed in the log-domain. In this relation, inaccuracy is mainly due to the shadowing impact, which increases linearly with the distance (a constant error in the log-distance implies a constant multiplicative error in the distance) and to the multipath (in particular for indoor scenarios) where RSSI fluctuations cannot be predicted by deterministic theoretical models. Thus, the measured power is

$$P_r(\mathrm{dBm}) = P_{\mathrm{ref}}(\mathrm{dBm}) - n_p \cdot 10\log_{10}\left(\frac{d}{d_{\mathrm{ref}}}\right) + n, \quad (1)$$

where P_{ref} is the power received at the reference distance d_{ref}, n_p is the path loss exponent, and n is the random shadowing component, which is Gaussian and zero-mean (in dB). We can adapt this model to our scenario by setting n_p and, given the lack of large structures such as buildings or trees, the channel model that fits best the scenario is the two-ray ground reflection. This model is validated by the real measurements taken in the field.

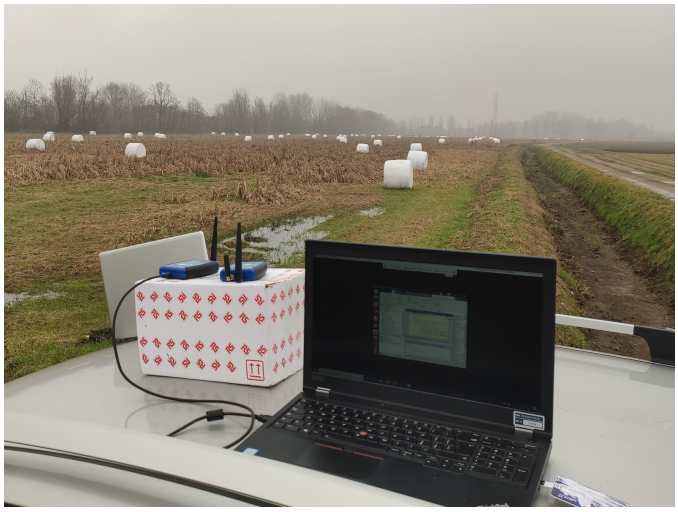

Fig. 1: Experimental setup of the ground-to-air link. There are two ADALM-Pluto SDRs on the roof of a car: one is the transmitter and the other is used for monitoring.

B. Proposed Threshold-based Approach

To improve the accuracy of the ML localization algorithm, a pre-processing phase can refine the raw data and reduce the impact of noise and interference [17]. In this paper, we are using an approach based on the definition of lower and upper thresholds to make the data usable. For the initial measurements, the UAV is close to the transmitter, as shown on the roof of the car in Fig. 1, and there is also human interference before the take off and multipath reflections. Therefore, the measurements when the UAV is close to the transmitter are neglected and an upper threshold of -50 dB is used for this aim. RSSI measurements lower than a certain value are also discarded because from our experiments we have found that they are comparable to the SDR noise floor. The lower and upper thresholds were derived empirically from the measures as discussed in Sec. IV.

C. Maximum Likelihood Algorithm

In the considered scenario, each UAV position defines an Anchor Point (AP). Let $\mathbf{u}$ and $\mathbf{s}_i$ be the three-dimensional (3D) state vectors that give the coordinates of the active RF target and of the UAV associated with the ith RSSI measure, respectively. A single RSSI measurement ρ_i at position $\mathbf{s}_i$ is modelled as [18]

$$\rho_i = h_i(\mathbf{u}, \mathbf{s}_i) + n_i, \quad i = 1, \ldots, N_{AP}, \quad (2)$$

where N_{AP} is the number of APs, n_i is the zero-mean additive Gaussian noise with standard deviation σ_i, and

$$h_i(\mathbf{u}, \mathbf{s}_i) = P_{\mathrm{ref}} - n_p \cdot 10\log_{10}\frac{\|\mathbf{u} - \mathbf{s}_i\|}{d_{\mathrm{ref}}}, \quad (3)$$

is a non-linear function of the state vectors ($\mathbf{u}$,$\mathbf{s}_i$) obtained from (1) with $d = \|\mathbf{u} - \mathbf{s}_i\|$, being $\|\mathbf{v}\|$ the norm of the vector $\mathbf{v}$. Now, we want to estimate the position $\hat{\mathbf{u}}$ from the set

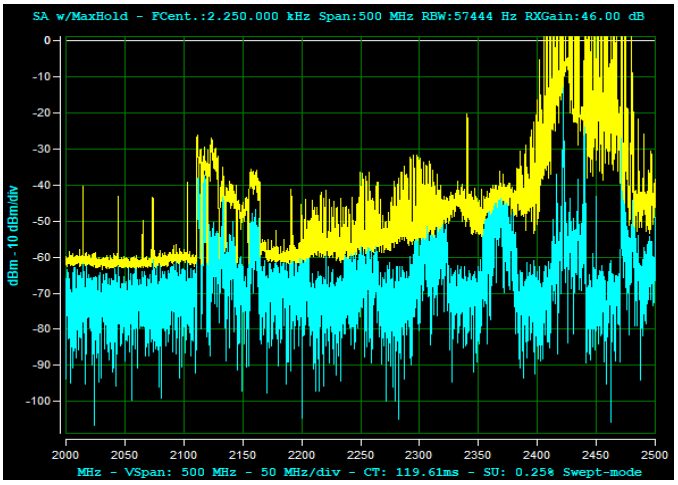

Fig. 2: The light blue signal is the drone controller transmission in the 2.4 GHz band and the yellow one is the max-hold of the received power. The frequency hopping nature of the transmission is the main cause of interference.

Fig. 3: The Tarot UAV in the complete configuration: we can see the ADALM Pluto SDR and the RaspberryPi with the SenseHat IMU board.

of measurements in (3) and this can be obtained by the ML estimation, as

$$\hat{\mathbf{u}}_{\mathbf{ML}} = \arg\max_{\mathbf{u}} \prod_{i=1}^{N_{AP}} \frac{1}{\sqrt{2\pi(\sigma_i)^2}} e^{-\left(\frac{\rho_i - h_i(\mathbf{u},\mathbf{s}_i)}{2\sigma_i}\right)^2}. \quad (4)$$

The absolute error is calculated as the distance between the true position of the transmitter and the ML estimation.

III. Experimental Measurement Campaign

For our experimental measurement campaign, we set up a simple and efficient architecture. For the ground segment, we placed a stable transmitter at the height of 1.7 m on the roof of a car, as shown in Fig. 1. The SDR used for transmission and reception is an ADALM-Pluto [16]. This board was selected for its light weight and wide frequency range, which allowed the collection of measures in both the 865 MHz [19] and 2.4 GHz bands.

The signal transmitted by the SDR is a QPSK modulated signal at the carrier frequency $f_c = 865$ MHz, in the first set of trials. This measurement campaign is used for the validation of the system, in absence of interference. Afterwards, we collected the same measures at $f_c = 2.4$ GHz, in presence of the interference. The interference was generated by the Wi-Fi hotspot and by the drone controller, as clearly shown by the light blue line in Fig. 2 reporting the intermittent transmission that causes interference. We have chosen these frequencies because they are part of the unlicensed spectrum and we can transmit with the SDR maximum available power, i.e., 7 dBm. Moreover, the two frequencies are close to those used in cellular communications and the result can be generalized even for this case. The QPSK modulated signal is sent to the SDR by a laptop running GNURadio, an open-source software used for digital signal processing [20]. For the receiver, the same SDR board was chosen and connected to a RaspberryPi 3B, installed on board a Tarot X6 Hexacopter. In Fig. 3, it is shown the complete setup of the drone, with the SDR and the RaspberryPi 3B. The choice of this minicomputer was driven by its light weight and sufficient computing power for our application. The RSSI value is computed directly by the SDR and we collected it with a GNURadio script that read the value every 10 ms, a sampling time achievable also with a low cost transceiver like the one described in [21]. The transceiver inside the ADALM-Pluto, the AD9361, measures first the power level in dB and then compensates for the receiver gain. Therefore, the collected value is valid also in case we are using an Adaptive Gain Control (AGC) system on the board. Since the board is not calibrated, the RSSI measure is not absolute but only relative and, for this reason, we took a calibration measure at 1 m of distance: this is used to estimate the values of all the gains at the receiver and match the relative RSSI measures to the actual values of path loss.

A. UAV Path Control

One fundamental aspect of the localization process is the definition of the flight path of the drone. An example of path optimization is reported in [22], where a set of way points that lay on a circle covering the area of interest is defined. The radius of the circle must be large enough to cover all the possible target locations but also kept as low as possible to reduce battery use. Some of the measures were acquired with programmed flight paths while some others were acquired with manual flight, to simulate both scenarios of autonomous and operator-controlled flights. In Fig. 4 it is shown the serpentine-like pattern we had programmed. To keep low the tilt angle of the drone we always moved it at a low controlled speed between 2 and 3 m/s. Moreover, the RSSI measuring interval of 10 ms corresponds to a space interval of $\Delta d = 2.3$ cm. With these values, we achieved a high spatial sampling frequency, which gave us also the possibility of averaging the measures.

The UAV flight telemetry may or may not be accessible, particularly during a flight, because the log file stored in the

Fig. 4: UAV flight track that was planned before the flight. Here we used a serpentine-like pattern covering the area of operations.

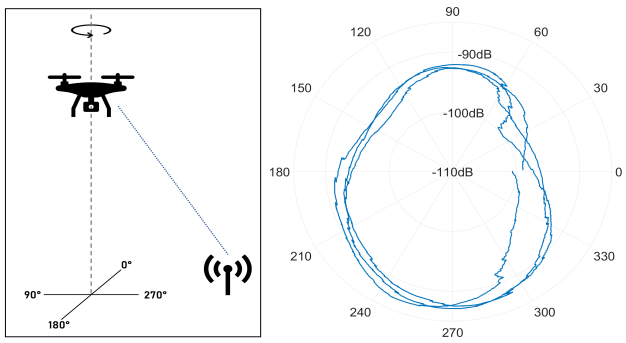

Fig. 5: Polar representation of the RSSI collected by the UAV while it was rotating around its vertical axis. We can clearly see how the variation of the bearing affects directly the RSSI, probably due to the shadowing caused by the drone itself.

drone is not always available. Therefore, attitude and position data were acquired utilizing an external add-on board to the Raspberry Pi mounted on the drone. For the attitude, we chose an Inertial Measuring Unit (IMU) board [23] capable of collecting pitch, yaw and roll angles using an accelerometer, gyroscope and compass. This sensor returns very noisy measures but we can still get a quite realistic representation of the attitude of the drone. In Fig. 5 we can visualize the effect of the bearing on the measured RSSI: by rotating the drone away from the transmitter we experience an instantaneous fading in the received power that follows exactly the trend of the yaw measure. This data can be of great help for the localization algorithm because we can compute the precise directivity of the antenna on board to weigh each collected RSSI sample. We remark that all the attitude data provided by the IMU board are relative angles w.r.t. the orientation at the start-up time. Furthermore, the same IMU board provides barometric measures, from which we computed the drone altitude with the barometric formula [24]. We have preferred this method in place of the straightforward GPS altitude because of the high fluctuations and low precision of the satellite 3D position [25], as represented in Fig. 6.

We consider the condition where the rate of variation of

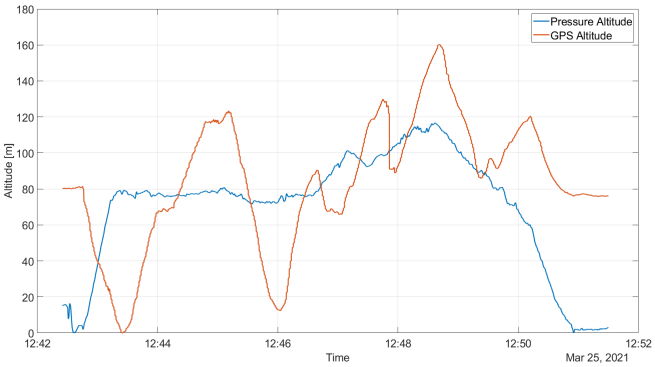

Fig. 6: Comparison between the altitude returned by the GPS and an estimate computed by the barometric sensor on the IMU. It is visible how the GPS altitude fluctuates around the more realistic values of the barometric altitude.

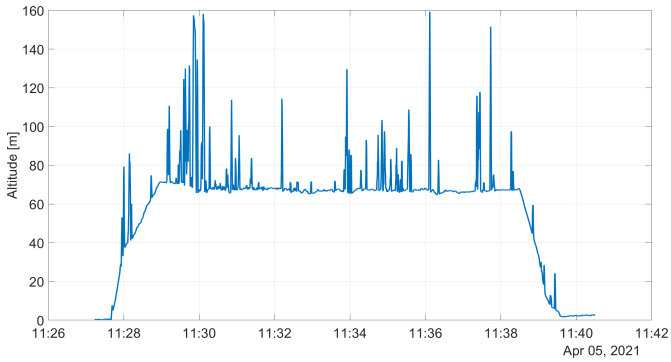

Fig. 7: The wind generated by the propellers causes spikes in the computed altitude.

temperature at increasing altitudes, known as *lapse rate*, is equal to zero because all the operations were carried out near to the ground. Thus, with this assumption, we can define the pressure at a given altitude h as

$$P(h) = P_{ref} \cdot \exp\left(-\frac{g_0 \cdot M \cdot (h - h_{ref})}{R^* \cdot T_{ref}}\right), \tag{5}$$

where $P_{ref}\,(\mathrm{Pa})$ is the reference pressure, $g_0\,(\mathrm{m/s^2})$ is the gravitational acceleration, $M\,(\mathrm{kg\,mol^{-1}})$ is the molar mass of Earth air, $h_{ref}\,(\mathrm{m})$ is the reference height, $R^*\,(\mathrm{J/(mol \cdot K)})$ is the universal gas constant, and $T_{ref}\,(\mathrm{K})$ is the reference temperature. If we define the auxiliary constant C as

$$C = -\frac{g_0 \cdot M}{R^* \cdot T_{ref}}, \tag{6}$$

it is possible to write the altitude variation from the reference as a function of the pressure change, which is given by

$$h(P) = \frac{\ln\left(P/P_{ref}\right)}{C}. \tag{7}$$

Therefore, by recording the maximum value of pressure on the ground as the reference we can compute a precise value of the altitude variation. However, the resulting altitude measure could be affected by the wind. In Fig. 7 we can see the spikes in the computed altitude, which are the effect of sudden changes in the air pressure. Indeed, the IMU board senses also

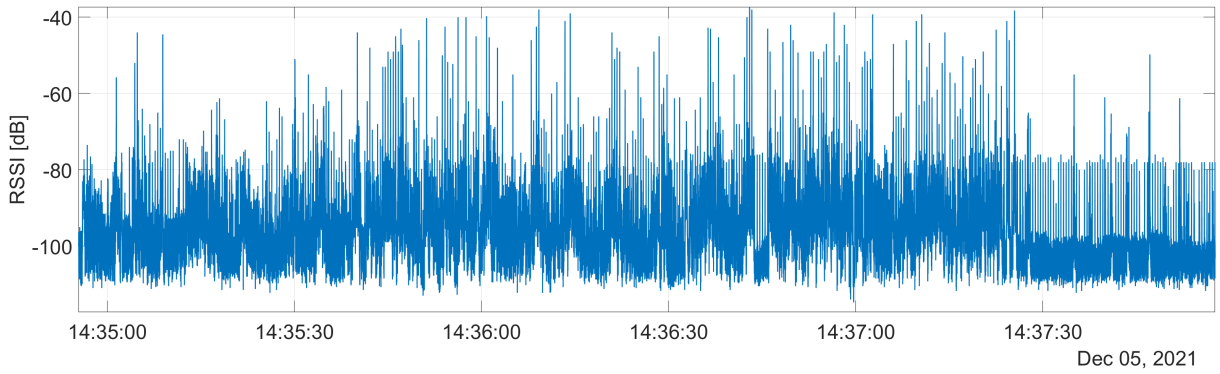

Fig. 8: Example of collected RSSI measures with interference.

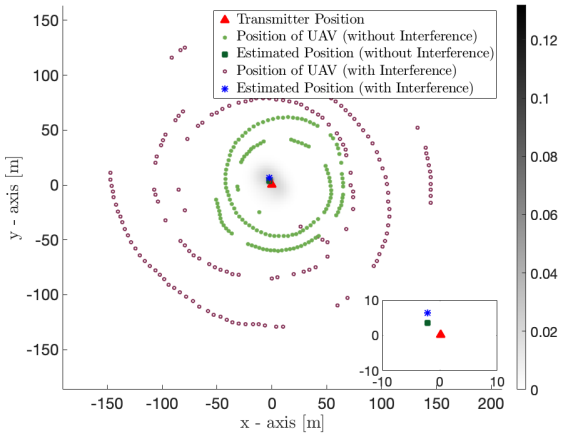

Fig. 9: ML estimation of the transmitter position with and w/o interference for the shown circular UAV flights.

the wind generated by UAV propellers and it is necessary to mount the board upside down in order to limit this problem.

For evaluating the error in the 2D position, we used an external GPS dongle [25] that provides also altitude, even if highly unreliable compared to the barometric one. The position accuracy of the 2D estimate is around 2.5 m but really depends on the number of satellites visible at the time of the trial.

IV. Localization Results

Here, we present the results of the ML localization algorithm obtained from the collected RSSI measurements without interference at 865 MHz and with interference at 2.4 GHz. For the estimation of the transmitter position, we used $n_p = 2.2$ in (1), which was empirically derived. Essentially, the scenario is that of a two rays channel, i.e. line-of-sight plus a reflection from the ground, with transmitter placed on the rooftop of a car. An example of RSSI values that were gathered in presence of interference is reported in Fig. 8. The RSSI is logged every 10 ms while the position twice per second. From data collected in our experiments, both without and with interference, we obtained a standard deviation between 2 and 6 dB from the estimated mean value associated with multiple measurements taken in each position, which gives the value of σ_i to be used in (4). The measured RSSI exhibits fluctuations that affect the accuracy of localization. Therefore, to improve the performance, and reduce the load on the localization algorithm at the same time, only a subset, i.e. the most reliable, of the RSSI measurements obtained by the UAV in different positions must be considered. These are obtained by thresholding RSSI between a lower and upper value (see Sec. II.B).

Figure 9 reports an example of the estimated position after the application of ML algorithm with RSSI thresholding for two circular tracks with and without interference. Here, the same value $\hat{\sigma}_i = 4$ dB, $i = 1, \ldots, N_{AP}$, was used in (4), which was obtained as mid way of the estimated standard deviation in the range $(4 - 6$ dB) observed from the collected RSSI. We can observe which UAV APs are considered for the localization after the threshold-based approach, visible in the figure as green and purple points, for the experimental tests without and with interference respectively. The circular track is an effective path for localization as there are measurements from all the directions. The numeric values of the likelihood associated with different estimated positions of the target are shown according to the grey scale reported on the right of the figure. The mean of the absolute location error is 4 m when there is no interference while it increases to 4.8 m with interference. This absolute error mean value is less than a meter worse than the best localization error without interference. Table I reports a summary of the results obtained in different experimental tests for the circular and serpentine tracks, shown in Fig. 4, together with the values used for the lower and upper thresholds. From the reported results we can observe that the presence of interference does not introduce significant degradation compared to the case where it is absent.

A. Multiple Transmitters

In order to verify the performance of our algorithm also in case of multiple ground transmitters, we collected measures in presence of 3 different transmitters positioned in an area of 300 m $\times$ 300 m. For this case, a serpentine track was used. We adapted the original algorithm for working in this new scenario, just by slicing the full set of recorded samples into 3 clusters. The slicing was done by analyzing the RSSI values and finding hot spots in the UAV track that suggested the presence of a transmitter. In this case we set $\hat{\sigma}_i = 6$ dB from

TABLE I: RSSI range (thresholds) and mean absolute position error for circular and serpentine tracks.

RSSI Thresholds (upper and lower)	Mean Absolute Position Error			
	Circ. w\Int.	Serp. w\Int.	Circ. No Int.	Serp. No Int.
-50 to -90 dBm	7 m	17 m	5.1 m	11.3 m
-50 to -95 dBm	5.5 m	14 m	4.1 m	16.4 m
-50 to -100 dBm	7.2 m	19 m	9.5 m	17.0 m
-50 to -105 dBm	10.8 m	14 m	12.2 m	16.5 m
-60 to -90 dBm	6.7 m	17.7 m	5.1 m	10.2 m
-70 to -90 dBm	6.1 m	16.7 m	5.1 m	16.4 m
-70 to -100 dBm	7.1 m	10.5 m	9.4 m	17.1 m
-70 to -110 dBm	12.9 m	13.2 m	12.3 m	16.2 m

the observation of the standard deviation in raw RSSI data associated with the considered serpentine path. Then, the localization procedure is applied in the 3 clusters independently and each result is merged. Figure 10 represents the estimated positions returned by the ML algorithm.

V. Conclusions and Future Work

In this paper we have considered the application of the ML algorithm for localizing an active RF transmitted from RSSI measures collected by a UAV in two unlicensed frequency bands. An experimental setup that uses inexpensive and lightweight ADALM Pluto SDR development board, programmed with the open-source software GNU Radio was described. Circular and serpentine tracks have been considered as trajectories for the UAV. The performance has been evaluated in terms of mean absolute position error either without interference at 865 MHz or with interference at 2.4 GHz. A threshold-based solution on the measured RSSI inputs has been proposed to improve the accuracy of the estimates. Our results show that the performance in presence of interference at 2.4 GHz is comparable to the scenario without interference at 865 MHz. The applicability of this approach to a multi-transmitter case has been demonstrated for a scenario with three RF emitters, in which a good accuracy is achieved.

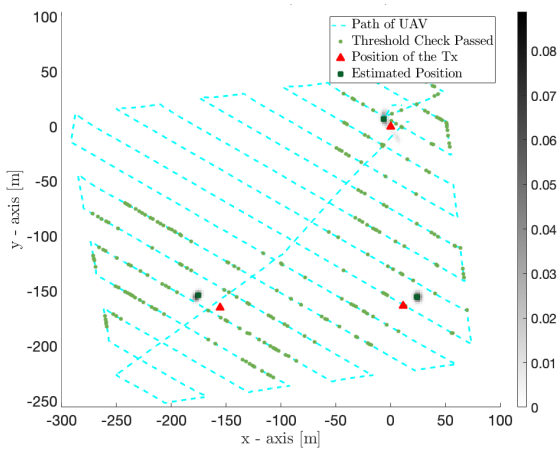

Fig. 10: Transmitter position estimation with a serpentine UAV flight, with three transmitters on the ground. The numeric values of the likelihood are represented in a grey scale, while the red triangles are the actual transmitter locations.

References

[1] A. Masood *et al.*, "Surveying pervasive public safety communication technologies in the context of terrorist attacks," *Phys. Commun.*, vol. 41, p. 101109, 2020.

[2] S. Tang *et al.*, "Study on RSS/AOA hybrid localization in life detection in huge disaster situation," *Natural Hazards*, vol. 95, pp. 569–583, 2019.

[3] F. Maurelli, S. Krupiński, X. Xiang, and Y. Petillot, "AUV localisation: a review of passive and active techniques," *Inter. J. Intell. Robotics Appl.*, pp. 1–24, 2021.

[4] H. P. Mistry and N. H. Mistry, "RSSI based localization scheme in wireless sensor networks: a survey," in *Proc. 5th Int. Conf. Adv. Comput. Commun. Technol.* IEEE, 2015, pp. 647–652.

[5] B. Xiang *et al.*, "UAV assisted localization scheme of WSNs using RSSI and CSI information," in *Proc. Int. Conf. Comput. Commun.*, 2020, pp. 718–722.

[6] M. Hasanzade *et al.*, "Localization and tracking of RF emitting targets with multiple unmanned aerial vehicles in large scale environments with uncertain transmitter power," in *Int. Conf. Unmanned Aircraft Syst.*, 2017, pp. 1058–1065.

[7] S. Shue, L. E. Johnson, and J. M. Conrad, "Utilization of XBee ZigBee modules and MATLAB for RSSI localization applications," in *Proc. SoutheastCon*, 2017, pp. 1–6.

[8] G. Wang, H. Chen, Y. Li, and N. Ansari, "NLOS error mitigation for TOA-based localization via convex relaxation," *IEEE Trans. Wireless Commun.*, vol. 13, pp. 4119–4131, 2014.

[9] Y. Liu, F. Guo, L. Yang, and W. Jiang, "An improved algebraic solution for TDOA localization with sensor position errors," *IEEE Commun. Lett.*, vol. 19, no. 12, pp. 2218–2221, 2015.

[10] H.-J. Shao, X.-P. Zhang, and Z. Wang, "Efficient closed-form algorithms for AOA based self-localization of sensor nodes using auxiliary variables," *IEEE Trans. Signal Process.*, vol. 62, pp. 2580–2594, 2014.

[11] S. M. M. Dehghan, H. Moradi, and S. A. A. Shahidian, "Optimal path planning for DRSSI based localization of an RF source by multiple uavs," in *Proc. RSI/ISM Int. Conf. Robot. Mechatronics*, 2014, pp. 558–563.

[12] S. Nagaraju, L. J. Gudino, B. V. Kadam, R. Ookalkar, and S. Udeshi, "RSSI based indoor localization with interference avoidance for wireless sensor networks using anchor node with sector antennas," in *Proc. Int. Conf. Wireless Commun. Signal Proc. Netw.*, 2016, pp. 2233–2237.

[13] D. Konings *et al.*, "The effects of interference on the RSSI values of a zigbee based indoor localization system," in *Proc. Int. Conf. Mechatronics Mach. Vision Pract.*, 2017, pp. 1–5.

[14] L. K. Dressel and M. J. Kochenderfer, "Efficient and low-cost localization of radio signals with a multirotor UAV," in *Proc. AIAA Guidance, Navig. Control Conf.*, 2018, p. 1845.

[15] M. Petitjean, S. Mezhoud, and F. Quitin, "Fast localization of ground-based mobile terminals with a transceiver-equipped UAV," in *Proc. 29th Int. Symp. Pers. Indoor Mob. Radio Commun.*, 2018, pp. 323–327.

[16] Analog Devices Inc, "PlutoSDR Wiki Page," [Online]. Available:: https://wiki.analog.com/university/tools/pluto, accessed: 31/12/2021.

[17] C. M. Judd, G. H. McClelland, and C. S. Ryan, *Data analysis: A model comparison approach*. Routledge, 2011.

[18] A. Patri and S. P. Rath, "Elimination of gaussian noise using entropy function for a RSSI based localization," in *Proc. Intern. Conf. Image Inf. Process.*, 2013, pp. 690–694.

[19] M. Saelens *et al.*, "Impact of EU duty cycle and transmission power limitations for sub-GHz LPWAN SRDs: An overview and future challenges," *Eurasip J. Wirel. Commun. Netw.*, pp. 1–32, 2019.

[20] "GNU Radio project," [Online]. Available: https://www.gnuradio.org/.

[21] Texas Instrument, "Low-Cost Low-Power 2.4 GHz RF Transceiver," [Online]. Available: https://bit.ly/3Ct9yvf, accessed: 9/3/2021.

[22] H. Sallouha, M. M. Azari, and S. Pollin, "Energy-constrained UAV trajectory design for ground node localization," in *Proc. IEEE GLOBECOM*, 2018, pp. 1–7.

[23] Raspberry Pi Foundation, "SenseHat Board," [Online]. Available: https://www.raspberrypi.org/products/sense-hat/, accessed: 31/12/2021.

[24] Berberan-Santos *et al.*, "On the barometric formula inside the earth," *J. Math. Chem.*, vol. 47, pp. 990–1004, 2010.

[25] U-blox, "GPS Dongle Documentation," [Online]. Available: https://bit.ly/3EGPgxY, accessed: 1/2/2021.